

Phase Control of Majorana Bound States in a Topological X Junction

Tong Zhou^{1,*}, Matthieu C. Dartailh^{1,2}, William Mayer,² Jong E. Han,¹
Alex Matos-Abiague,³ Javad Shabani,² and Igor Žutić^{1,†}

¹Department of Physics, University at Buffalo, State University of New York, Buffalo, New York 14260, USA

²Center for Quantum Phenomena, Department of Physics, New York University, New York, New York 10003, USA

³Department of Physics and Astronomy, Wayne State University, Detroit, Michigan 48201, USA



(Received 8 September 2019; accepted 19 February 2020; published 1 April 2020)

Topological superconductivity supports exotic Majorana bound states (MBS) which are chargeless zero-energy emergent quasiparticles. With their non-Abelian exchange statistics and fractionalization of a single electron stored nonlocally as a spatially separated MBS, they are particularly suitable for implementing fault-tolerant topological quantum computing. While realizing MBS has focused on one-dimensional systems, the onset of topological superconductivity requires delicate parameter tuning and geometric constraints pose significant challenges for their control and demonstration of non-Abelian statistics. To overcome these challenges, building on recent experiments in planar Josephson junctions (JJs), we propose a MBS platform of X-shaped JJs. This versatile implementation reveals how external flux control of the superconducting phase difference can generate and manipulate multiple MBS pairs to probe non-Abelian statistics. The underlying topological superconductivity exists over a large parameter space, consistent with materials used in our fabrication of such X junctions, as an important step towards scalable topological quantum computing.

DOI: 10.1103/PhysRevLett.124.137001

Majorana bound states (MBS), which are their own antiparticles [1], are usually sought in proximity-modified materials [2–7]. This approach overcomes the need for native spinless p -wave superconductivity, whose existence is debated even among the leading candidates such as Sr_2RuO_4 [8,9]. Early MBS proposals have focused on proximity effects in one-dimensional (1D) geometries [10–13]. However, they rely on signatures, such as a quantized zero-bias peak [14,15], which do not probe the non-Abelian statistics crucial for implementing topological quantum computing [16,17]. These 1D platforms also pose inherent difficulties for MBS braiding.

A push to seek alternative platforms for topological superconductivity led to the demonstration of robust proximity-induced superconductivity in a two-dimensional electron gas (2DEG) [18–20] which offers important opportunities to realize and control MBS [21–29]. Recent experiments in planar Josephson junctions (JJs) [30–32] reveal that topological superconductivity exists over a large parameter space without requiring fine tuning, while demonstrating the key role of a superconducting phase to control the topological transition.

In this work we propose topological X-shaped junctions (XJs) as a natural 2D generalization of planar JJs, based on common normal (N) and superconducting (S) regions, to realize multiple MBS pairs and enable probing non-Abelian statistics. The setup is shown in Fig. 1(a). Four S films (Al) on the top of a 2DEG (InAs) form an X-shaped channel with the angle of 2θ , defined between the S leads.

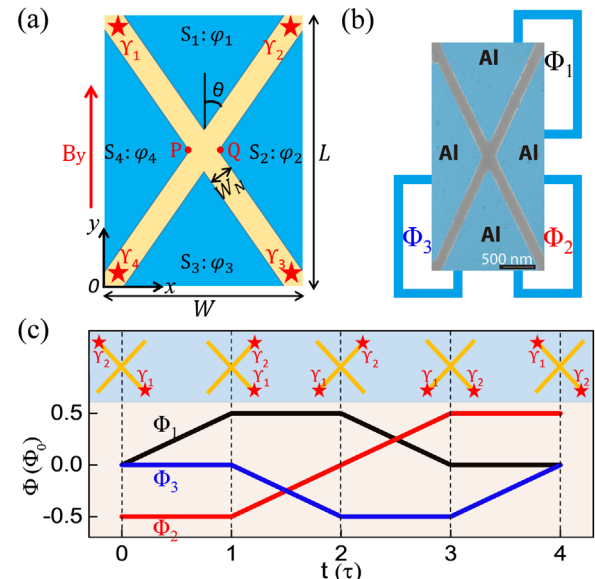


FIG. 1. (a) X junction (XJ) schematic formed by epitaxial superconducting (S) regions (blue) covering a 2DEG (yellow). A crossed X channel with the angle of 2θ , defined between the S leads, can be tuned into the topological regime with MBS $\gamma_1, \dots, \gamma_4$ (stars) at its ends by the phase differences among the S regions with an in-plane magnetic field along y direction. All MBS pair combinations are obtained through modulating the phase differences between $\varphi_1, \varphi_2, \varphi_3$, and φ_4 . (b) SEM image for the XJ with schematic external fluxes Φ_1 (between S_1, S_2), $\Phi_2(S_2, S_3)$, and $\Phi_3(S_3, S_4)$. (c) MBS exchange with fluxes, τ is the switching time, and Φ_0 is the magnetic flux quantum.

Such an XJ, with an in-plane magnetic field, \mathbf{B} , along the y direction, can be tuned into the topological regime by controlling the phase differences among the four S regions ($\varphi_1, \dots, \varphi_4$), where either MBS pairs or MBS quadruplet are formed at the XJ's ends.

Experimentally, as seen from the scanning electron microscope image in Fig. 1(b), XJs can be fabricated and patterned easily using standard electron beam lithography by selectively removing Al. This technique was successful for fabrication of superconducting-normal and Josephson junctions [32,33]. The top-down approach of XJs allows arbitrary design dimensions while keeping the channel between S electrodes less than the 2DEG's mean free path (within 100 nm for parameters considered). With the three flux loops [Fig. 1(b)], the phases between the four S regions can be tuned to enable moving and exchanging MBS. We show schematically exchanging MBS with the flux-control of Φ_1 , Φ_2 , and Φ_3 in Fig. 1(c).

In the previous work on planar JJs, the focus was on \mathbf{B} applied along the superconducting-normal interface to realize MBS [21,30]. However, to support multiple MBS in XJs, the topological superconductivity should survive when the in-plane \mathbf{B} deviates from that direction, just as B_y in Fig. 1(a) is no longer along the superconducting-normal interface, forming the misalignment angle = θ , discussed in Ref. [34]. For a single JJ, our calculation shows that the phase-difference range supporting MBS becomes smaller when the misalignment angle increased, but even up to 0.15π , there is still a finite phase-difference range (0.58π to 1.16π) for topological states [34]. As the misalignment angle increases, the topological region is reduced and, eventually, fully suppressed [34], as observed experimentally [32].

The MBS robustness in a single JJ against \mathbf{B} misalignment angle $< 0.2\pi$ provides guidance to design XJs [34]. We expect that XJs would support multiple MBS for $\theta < 0.2\pi$ with the applied B_y , as shown in Fig. 1(a). The XJ can be viewed as including four planar JJs: $S_1/N/S_2$, $S_2/N/S_3$, $S_3/N/S_4$, and $S_4/N/S_1$. For each JJ, changing the phase difference from 0 to ϕ_0 (ϕ_0 is studied in Fig. 2) results in a corresponding transition from trivial to topological junction with MBS at its ends.

At the XJ's center, common to individual JJs, MBS can be fused. We distinguish their three types: short-edge (γ_3, γ_4) with the phases $(\varphi_1, \varphi_2, \varphi_3, \varphi_4) = (0, 0, \phi_0, 0)$, long-edge (γ_2, γ_3) with $(0, \phi_0, 0, 0)$, and diagonal (γ_1, γ_3) with $(\phi_0, \phi_0, 0, 0)$, as shown in Fig. 1(a). To study MBS control and identify the ϕ_0 supporting topological states, in our calculations we use the Bogoliubov-de Gennes (BdG) Hamiltonian,

$$H = \left[\frac{\mathbf{p}^2}{2m^*} - \mu(x, y) + \frac{\alpha}{\hbar} (p_y \sigma_x - p_x \sigma_y) \right] \tau_z - \frac{g^* \mu_B}{2} \mathbf{B} \cdot \boldsymbol{\sigma} + \Delta(x, y) \tau_+ + \Delta^*(x, y) \tau_-, \quad (1)$$

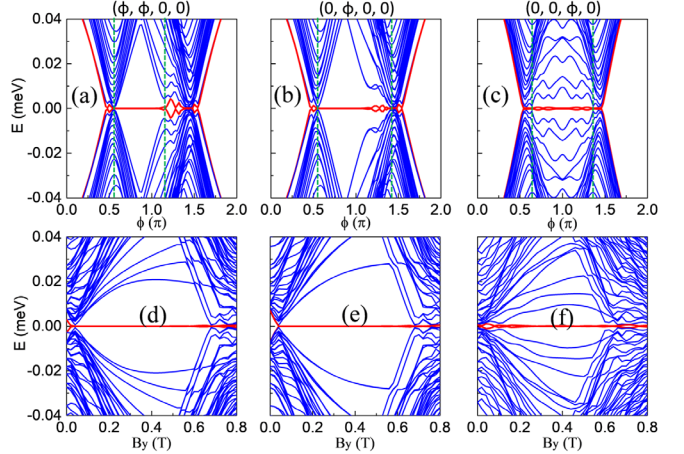


FIG. 2. (a)–(c) Energy spectra at $B_y = 0.4$ T as a function of ϕ for the diagonal, long- and short-edge MBS in the XJ with half-central angle $\theta = 0.1\pi$, as seen in Fig. 1. Red lines: evolution of finite-energy states into MBS inside the topological gap. The ϕ values between the two green lines (ϕ_0) give the topologically nontrivial states. (d)–(f) Magnetic field dependence of the energy spectrum with superconducting phases $(\varphi_1, \dots, \varphi_4) = (\pi, \pi, 0, 0)$, $(0, \pi, 0, 0)$, and $(0, 0, \pi, 0)$, respectively. The red lines retain the meaning as in (a)–(c). The materials and geometry parameters are specified in the main text.

numerically solving the corresponding eigenvalue problem on a discretized lattice as implemented in KWANT [35]. Here \mathbf{p} is the momentum, $\mu(x, y)$ is the chemical potential, α is the Rashba spin-orbit coupling (SOC) strength, \mathbf{B} is the external magnetic field, μ_B is the Bohr magneton, while m^* and g^* are the electron effective mass and g factor, respectively. We use $\tau_i(\sigma_i)$ as the Nambu (Pauli) matrices in particle-hole (spin) space and $\tau_{\pm} = (\tau_x \pm i\tau_y)/2$. $\Delta(x, y)$ is the proximity-induced superconducting pair potential, for the 2DEG below the S leads S_n ($n = 1, \dots, 4$), it can be expressed, using the BCS relation for the B -field suppression, as

$$\Delta(x, y) = \Delta_0 \sqrt{1 - (B/B_c)^2} e^{i\varphi_n}, \quad (2)$$

where Δ_0 is the superconducting gap, B_c is the critical magnetic field, and φ_n is the corresponding superconducting phase. The S and N regions are simply expressed using the coordinates of the points P and Q in Fig. 1(a). For example,

$$S_1(x, y) = \begin{cases} y > \cot \theta(x - x_P) + y_P \\ y > -\cot \theta(x - x_Q) + y_Q \end{cases}, \quad (3)$$

where $x_{P,Q} = (W \mp W_N / \cos \theta)/2$, $y_{P,Q} = L/2$. The other S and N regions are explicitly given in Ref. [34]. We choose

material parameters consistent with our fabricated XJs [Fig. 1(b)] that also match experimental observation of robust proximity-induced superconductivity and topological states in epitaxial Al/InAs-based JJs [32], $m^* = 0.03m_0$, where m_0 is the electron mass, and $g^* = 10$ for InAs, $\Delta_0 = 0.23$ meV, $\alpha = 10$ meV nm, $B_c = 1.6$ T, and for the N , S chemical potential $\mu_S = \mu_N = 0.5$ meV. We consider XJs with $L = 3.2$ μm , $W = L/2$, $W_N \approx 100$ nm, and Al/InAs material parameters in Figs. 2–4.

It is instructive to examine the robustness of the topological states as a function of ϕ for the diagonal, long- and short-edge MBS, shown in Figs. 2(a)–2(c), respectively. The evolution of the lowest-energy states into MBS reveals a large range of $\phi_0 \in (0.6\pi, 1.2\pi)$ for diagonal, $(0.6\pi, 1.4\pi)$ for long-edge, and $(0.64\pi, 1.36\pi)$ for short-edge MBS. Since the geometry for diagonal MBS ($\varphi_1 = \varphi_2 = \phi$, and $\varphi_3 = \varphi_4 = 0$) resembles the single JJ with the B -field misalignment θ , we also expect the similarities in their spectra. Indeed, for $\theta = 0.1\pi$ this can be seen in Ref. [34].

The results from Figs. 2(a)–2(c) suggest that, as in a single JJ [21], the choice $\phi_0 = \pi$ is particularly desirable for the stability of the topological state and could reduce the critical field for the onset of MBS in XJs. For such $\phi_0 = \pi$ we also examine complementary information about the robustness of topological states with in-plane B_y . From the low-energy spectra in Figs. 2(d)–2(f), we see that, similar to the single JJ, a small $B_y \sim 0.1$ T already supports all three MBS types. As expected from MBS in short 1D systems, for the short edge [Fig. 2(f)] the topological gap is the smallest and its zero energy bands have small oscillations which can be suppressed with an increased system size [34,36–39].

While our previous results are encouraging, suggesting that different MBS could be supported in XJs, they all considered a fixed half-angle between the two N regions, $\theta = 0.1\pi$, which could be challenging to exactly replicate experimentally. It is therefore important to identify the θ range still allowing these topological states. With the fixed system size ($L = 3.2$ μm , $W = L/2$, and $W_N \approx 100$ nm) in Ref. [34] we calculate θ -dependent energy spectra for different MBS. When $\theta \sim 0$ the diagonal and long-edge configuration can be approximated as a single π -JJ where the MBS are stable up to a misalignment angle $\sim 0.2\pi$ of the B field away from the N/S interface. Indeed, when related XJs are calculated we find that these two MBS types are supported for $\theta \lesssim 0.18\pi$. However, for short-edge MBS and $\theta \sim 0$, the areas of S_1 and S_3 are too small to support such MBS. Instead, MBS emerge at $\theta \approx 0.08\pi$ and remain stable for $\theta \lesssim 0.18\pi$ [34].

With these results, we can identify that all the three MBS types can coexist in a robust form for $\theta \in (0.08\pi, 0.18\pi)$ with $L \geq 3.2$ μm and $W \geq 1.6$ μm . Such a large parameter range gives a considerable flexibility for XJ fabrication.

Our fabricated XJ [Fig. 1(b)] already fits well in this range of suitable geometric parameters, with $L = 4.0$ μm , $W = 2.0$ μm , and $\theta = 0.15\pi$.

The existence of MBS is an important precondition, but alone does not ensure their successful manipulation in XJs which could offer an important generalization of the previous planar JJs to a much more versatile 2D platform. We therefore consider in detail the scheme for phase control of MBS with three external fluxes sketched in Fig. 1(c) such that flux in one of the four S regions is changed within the switching time, 0.2 ns $< \tau \sim 1$ μs . The lower and upper limits are given by the uncertainty relation using the smallest calculated energy gap ~ 2 μeV to the first excited state [34] and the quasiparticle poisoning time [40–42], respectively.

Since two MBS can exist at any two ends of the XJ with the specific phase differences, it gives us a chance to realize MBS exchange and fusion using the phase control. To describe the MBS exchange of γ_1 and γ_2 in XJs, we plot schematically their evolution in Figs. 3(a)–3(e).

Initially, at $t = 0$, diagonal MBS (γ_1, γ_2) are located at the opposite corners, depicted in Fig. 3(a), by setting the three fluxes (Φ_1, Φ_2, Φ_3) as $(0, -0.5\Phi_0, 0)$. First, γ_2 is moved to the upper-right corner to form the long-edge MBS shown in Fig. 3(b) by changing Φ_1 from 0 to $0.5\Phi_0$ at $t = \tau$. The feasibility of this process is verified by calculating the adiabatic evolution of the MBS probability densities, shown in Figs. 3(f)–3(j), for the realistic Al/InAs parameters from Fig. 2 at $B_y = 0.2$ T. During the switching time τ , when the phase difference φ_1 changes continuously from 0 to $\phi_0 = \pi$, well-localized MBS are protected by the topological superconducting gap such that γ_2 can be adiabatically moved from the upper-left to the upper-right corner through the XJ center [34].

In the next step, γ_1 is moved from the lower-right to the lower-left corner in Fig. 3(c) by changing (Φ_2, Φ_3) from $(-0.5\Phi_0, 0)$ to $(0, -0.5\Phi_0)$ at $t = 2\tau$. This process changes the long-edge to a diagonal MBS, which can, because of the mirror symmetry in the XJ, be viewed as equivalent to the transition from Figs. 3(b) to 3(a). The following step is to move γ_2 from the upper-right to the lower-right corner in Fig. 3(d) by changing (Φ_1, Φ_2) from $(0.5\Phi_0, 0)$ to $(0, 0.5\Phi_0)$ at $t = 3\tau$. Changing the diagonal to a short-edge MBS is verified by calculating the MBS probability densities, shown in Figs. 3(k)–3(o), where the phase difference φ_2 changes from π to 0. We can see the MBS are robust and γ_2 can be adiabatically moved to the original position of γ_1 . Finally, γ_1 is moved from the lower-left to the upper-left corner in Fig. 3(e) by changing Φ_3 from $-0.5\Phi_0$ to 0 at $t = 4\tau$. This process, due to the mirror symmetry in the XJ, is equivalent to the transition from Fig. 3(d) to 3(c), where γ_1 is moved to the original position of γ_2 . Through these four switching steps (from $t = 0$ to $t = 4\tau$), γ_1 and γ_2 are adiabatically exchanged. Further information about this exchange, including related movies, is in Ref. [34].

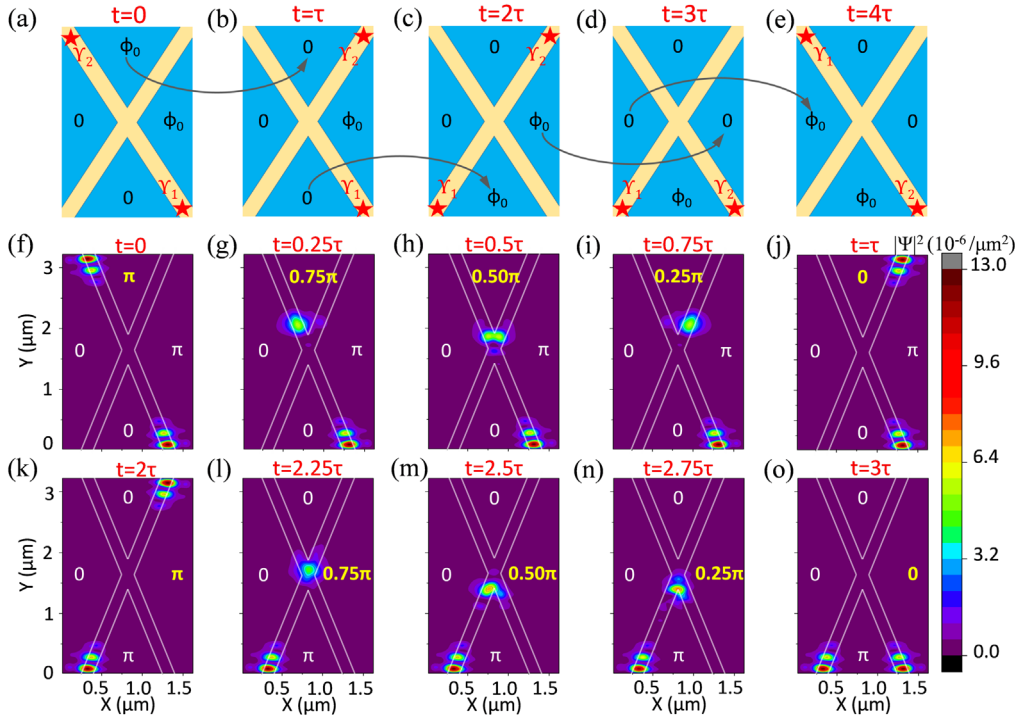


FIG. 3. (a)–(e) Schematic of exchanging MBS in the XJ with external flux control, following the protocol from Fig. 1(c). ϕ_0 is the phase difference supporting all three MBS types shown in Fig. 2. (f)–(j) Evolution of the calculated MBS probability densities from the diagonal (a) to a long-edge MBS (b) through continuously changing φ_1 from π to 0, but fixing $\varphi_2 = \pi$, $\varphi_3 = 0$, and $\varphi_4 = 0$. (k)–(o) Evolution of the calculated MBS probability densities from diagonal (c) to short-edge MBS (d) by changing φ_2 from π to 0, but fixing $\varphi_1 = 0$, $\varphi_3 = \pi$, and $\varphi_4 = 0$. It is not important if the corners do not coincide with the ends of diagonals. The Al/InAs parameters are taken from Fig. 2 with $B_y = 0.2$ T.

Our proposed XJs can be used to explore the MBS fusion rules [17]. For example, starting from the diagonal MBS, γ_1 and γ_2 can be gradually moved and fused at the center of the XJ by using the three external fluxes to change φ_1 from 0 to 0.5π , and then to change φ_3 from π to 0.5π , within the time 2τ . The corresponding evolution of the calculated MBS densities is shown in Ref. [34]. Since we find from Fig. 4 that four MBS can be generated, a more complex fusion in the XJ, for example, fusing (γ_1, γ_2) and fusing (γ_2, γ_3) , can access different fusion channels, which could probe non-Abelian statistics [17].

The versatility of the MBS phase control in 2D XJs also provides a powerful platform to implement braiding which requires at least four MBS. In a single XJ, as shown in Fig. 4(a), four MBS can be simultaneously realized at the four corners when $(\varphi_1, \varphi_2, \varphi_3, \varphi_4) = (\pi, 0, \pi, 0)$ set by the fluxes $(\Phi_1, \Phi_2, \Phi_3) = (-0.5\Phi_0, 0.5\Phi_0, -0.5\Phi_0)$. The presence of these MBS is verified from the calculated low-energy spectra in Fig. 4(b). The two MBS pairs exist within the topological gap for $B_y \in (0.1T, 0.6T)$. The corresponding wave function probability densities also clearly indicate in Fig. 4(c) that the formation of four MBS is localized at the four corners of the XJ. An important advantage of our platform is its scalability, using lithography, multiple XJs can be realized. In just two joint

XJs having six ends in the N regions at which MBS can be localized, with external fluxes and phase control fifteen different realizations of four MBS are possible.

While our work was motivated by the recent advanced in high-quality epitaxial Al/InAs junctions several of our findings have direct implications for other systems seeking to manipulate Majorana bound states. For example, state-of-the art fabrication of superconducting junctions with topological insulators [43] would support fabrication of

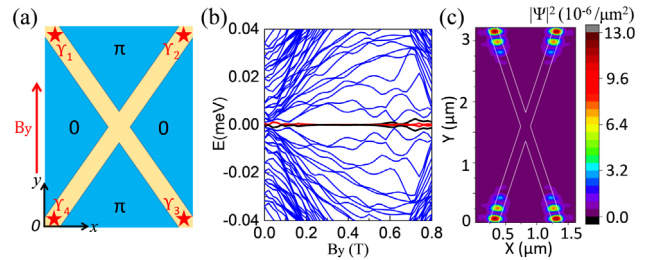


FIG. 4. (a) Schematic of four simultaneous MBS in the XJ with superconducting phases $(\varphi_1, \varphi_2, \varphi_3, \varphi_4) = (\pi, 0, \pi, 0)$. (b) Magnetic field dependence of the low-energy spectrum for (a). (c) Calculated probability densities for the two lowest-energy states in (b) with $B_y = 0.2$ T. The parameters are taken from Fig. 2.

similar X-shaped junctions. With the progress in tunable magnetic textures used to modify proximity-induced superconductivity [23,27,44–55], X-shaped junctions could be considered with a reduced role of an applied magnetic field.

Throughout our calculations the influence of the central angle 2θ between two superconducting-normal interfaces was emphasized, which could be further optimized [56]. While common approaches to realize exchanging and braiding envision structures such as the T -junction or crossbar geometries [57], we see their underlying right angles as detrimental to the robust manipulation of Majorana bound states. Instead, as in our X-shaped junctions, it is important to implement acute angles $2\theta < \pi/2$ in schemes relying on applied in-plane magnetic field. In an early work on multiple Josephson junctions with topological insulators [2] the situation is slightly better with the characteristics $\pi/3$ angle. However, that angle is still too large for junctions with more common materials, such as Al/InAs, using in-plane magnetic field. Experimental demonstration of the proposed two-dimensional manipulation of Majorana states in these topological X-shaped junctions would constitute an important milestone towards scalable topological quantum computing and stimulate further studies in the design of emergent phenomena in proximitized materials [58].

Tong Zhou would like to thank Avery Zhou for inspiration. We thank the referees for their valuable suggestions. This work is supported by DARPA Grant No. DP18AP900007, US ONR Grant No. N000141712793 (I. Ž. and A. M.-A.), NSF DMR Grant No. 1836687 (J. S.) and the UB Center for Computational Research.

- [8] A. P. Mackenzie and Y. Maeno, The superconductivity of Sr_2RuO_4 and the physics of spin-triplet pairing, *Rev. Mod. Phys.* **75**, 657 (2003).
- [9] I. Žutić and I. Mazin, Phase-Sensitive Tests of the Pairing State Symmetry in Sr_2RuO_4 , *Phys. Rev. Lett.* **95**, 217004 (2005).
- [10] V. Mourik, K. Zuo, S. M. Frolov, S. R. Plissard, E. P. A. M. Bakkers, and L. P. Kouwenhoven, Signatures of Majorana fermions in hybrid superconductor-semiconductor nanowire devices, *Science* **336**, 1003 (2012).
- [11] L. P. Rokhinson, X. Liu, and J. K. Furdyna, The factional a.c. Josephson effect in a semiconductor-superconductor nanowire as a signature of Majorana particles, *Nat. Phys.* **8**, 795 (2012).
- [12] M. T. Deng, C. L. Yu, G. Y. Huang, M. Larsson, P. Caroff, and H. Q. Xu, Anomalous zero-bias conductance peak in a Nb-InSb nanowire-Nb hybrid device, *Nano Lett.* **12**, 6414 (2012).
- [13] E. J. H. Lee, X. Jiang, R. Aguado, G. Katsaros, C. M. Lieber, and S. De Franceschi, Zero-Bias Anomaly in a Nanowire Quantum Dot Coupled to Superconductors, *Phys. Rev. Lett.* **109**, 186802 (2012).
- [14] K. Sengupta, I. Žutić, H.-J. Kwon, V. M. Yakovenko, and S. Das Sarma, Midgap edge states and pairing symmetry of quasi-one-dimensional organic superconductors, *Phys. Rev. B* **63**, 144531 (2001).
- [15] K. T. Law, P. A. Lee, and T. K. Ng, Majorana Fermion Induced Resonant Andreev Reflection, *Phys. Rev. Lett.* **103**, 237001 (2009).
- [16] C. Nayak, S. H. Simon, A. Stern, M. Freedman, and S. Das Sarma, Non-Abelian anyons and topological quantum computation, *Rev. Mod. Phys.* **80**, 1083 (2008).
- [17] D. Aasen, M. Hell, R. V. Mishmash, A. Higginbotham, J. Danon, M. Leijnse, T. S. Jespersen, J. A. Folk, C. M. Marcus, K. Flensberg, and J. Alicea, Milestones Toward Majorana-Based Quantum Computing, *Phys. Rev. X* **6**, 031016 (2016).
- [18] J. Shabani, M. Kjaergaard, H. J. Suominen, Y. Kim, F. Nichele, K. Pakrouski, T. Stankevic, R. M. Lutchyn, P. Krogstrup, R. Feidenhans'l, S. Kraemer, C. Nayak, M. Troyer, C. M. Marcus, and C. J. Palmstrøm, Two-dimensional epitaxial superconductor-semiconductor heterostructures: A platform for topological superconducting networks, *Phys. Rev. B* **93**, 155402 (2016).
- [19] W. Mayer, J. Yuan, K. S. Wickramasinghe, T. Nguyen, M. C. Dartiaih, and J. Shabani, Superconducting proximity effect in epitaxial Al-InAs heterostructures, *Appl. Phys. Lett.* **114**, 103104 (2019).
- [20] W. Mayer, M. C. Dartiaih, J. Yuan, K. S. Wickramasinghe, E. Rossi, and J. Shabani, Gate controlled anomalous phase shift in Al/InAs Josephson junctions, *Nat. Commun.* **11**, 212 (2020).
- [21] F. Pientka, A. Keselman, E. Berg, A. Yacoby, A. Stern, and B. I. Halperin, Topological Superconductivity in a Planar Josephson Junction, *Phys. Rev. X* **7**, 021032 (2017).
- [22] M. Hell, M. Leijnse, and K. Flensberg, Two-Dimensional Platform for Networks of Majorana Bound States, *Phys. Rev. Lett.* **118**, 107701 (2017).
- [23] G. L. Fatin, A. Matos-Abiague, B. Scharf, and I. Žutić, Wireless Majorana Bound States: From Magnetic Tunability to Braiding, *Phys. Rev. Lett.* **117**, 077002 (2016).

*tzhou8@buffalo.edu

†zigor@buffalo.edu

- [1] A. Yu Kitaev, Unpaired Majorana fermions in quantum wires, *Phys. Usp.* **44**, 131 (2001).
- [2] L. Fu and C. L. Kane, Superconducting Proximity Effect and Majorana Fermions at the Surface of a Topological Insulator, *Phys. Rev. Lett.* **100**, 096407 (2008).
- [3] R. M. Lutchyn, J. D. Sau, and S. Das Sarma, Majorana Fermions and a Topological Phase Transition in Semiconductor-Superconductor Heterostructures, *Phys. Rev. Lett.* **105**, 077001 (2010).
- [4] Y. Oreg, G. Refael, and F. von Oppen, Helical Liquids and Majorana Bound States in Quantum Wires, *Phys. Rev. Lett.* **105**, 177002 (2010).
- [5] J. Alicea, Majorana fermions in a tunable semiconductor device, *Phys. Rev. B* **81**, 125318 (2010).
- [6] J. Klinovaja, P. Stano, and D. Loss, Transition from Fractional to Majorana Fermions in Rashba Nanowires, *Phys. Rev. Lett.* **109**, 236801 (2012).
- [7] I. Žutić, A. Matos-Abiague, B. Scharf, H. Dery, and K. Belashchenko, Proxitized materials, *Mater. Today* **22**, 85 (2019).

- [24] A. Stern and E. Berg, Fractional Josephson Vortices and Braiding of Majorana Zero Modes in Planar Superconductor-Semiconductor Heterostructures, *Phys. Rev. Lett.* **122**, 107701 (2019).
- [25] B. Scharf, F. Pientka, H. Ren, A. Yacoby, and E. M. Hankiewicz, Tuning topological superconductivity in phase-controlled Josephson junctions with Rashba and Dresselhaus spin-orbit coupling, *Phys. Rev. B* **99**, 214503 (2019).
- [26] J. Liu, Y. Wu, Q.-F. Sun, and X. C. Xie, Flux-induced topological superconductor in planar Josephson junction, *Phys. Rev. B* **100**, 235131 (2019).
- [27] T. Zhou, N. Mohanta, J. E. Han, A. Matos-Abiague, and I. Žutić, Tunable magnetic textures in spin valves: From spintronics to Majorana bound states, *Phys. Rev. B* **99**, 134505 (2019).
- [28] F. Setiawan, A. Stern, and E. Berg, Topological superconductivity in planar Josephson junctions: Narrowing down to the nanowire limit, *Phys. Rev. B* **99**, 220506(R) (2019).
- [29] F. Setiawan, C.-T. Wu, and K. Levin, Full proximity treatment of topological superconductors in Josephson-junction architectures, *Phys. Rev. B* **99**, 174511 (2019).
- [30] A. Fornieri, A. M. Whiticar, F. Setiawan, E. Portolés, A. C. C. Drachmann, A. Keselman, S. Gronin, C. Thomas, T. Wang, R. Kallaher, G. C. Gardner, E. Berg, M. J. Manfra, A. Stern, C. M. Marcus, and F. Nichele, Evidence of topological superconductivity in planar Josephson junctions, *Nature (London)* **569**, 89 (2019).
- [31] H. Ren, F. Pientka, S. Hart, A. Pierce, M. Kosowsky, L. Lunczer, R. Schlereth, B. Scharf, E. M. Hankiewicz, L. W. Molenkamp, B. I. Halperin, and A. Yacoby, Topological superconductivity in a phase-controlled Josephson junction, *Nature (London)* **569**, 93 (2019).
- [32] W. Mayer, M. C. Dartailh, J. Yuan, K. S. Wickramasinghe, A. Matos-Abiague, I. Žutić, and J. Shabani, Phase signature of topological transition in Josephson junctions, *arXiv: 1906.01179*.
- [33] M. Kjaergaard, F. Nichele, H. J. Suominen, M. P. Nowak, M. Wimmer, A. R. Akhmerov, J. A. Folk, K. Flensberg, J. Shabani, C. J. Palmström, and C. M. Marcus, Majorana fermions in superconducting nanowires without spin-orbit coupling, *Nat. Commun.* **7**, 12841 (2016).
- [34] See Supplemental Material at <http://link.aps.org/supplemental/10.1103/PhysRevLett.124.137001> for the expanded discussion of the MBS robustness in planar JJs and XJs as well the process of the MBS exchange and fusion, supported by additional .gif files complementing Fig. 3.
- [35] C. W. Groth, M. Wimmer, A. R. Akhmerov, and X. Waintal, KWANT: A software package for quantum transport, *New J. Phys.* **16**, 063065 (2014).
- [36] J. S. Lim, L. Serra, R. López, and R. Aguado, Magnetic-field instability of Majorana modes in multiband semiconductor wires, *Phys. Rev. B* **86**, 121103(R) (2012).
- [37] E. Prada, P. San-Jose, and R. Aguado, Transport spectroscopy of NS nanowire junctions with Majorana fermions, *Phys. Rev. B* **86**, 180503(R) (2012).
- [38] S. Das Sarma, J. D. Sau, and T. D. Stanescu, Splitting of the zero-bias conductance peak as smoking gun evidence for the existence of the Majorana mode in a superconductor-semiconductor nanowire, *Phys. Rev. B* **86**, 220506(R) (2012).
- [39] D. Rainis, L. Trifunovic, J. Klinovaja, and D. Loss, Towards a realistic transport modeling in a superconducting nanowire with Majorana fermions, *Phys. Rev. B* **87**, 024515 (2013).
- [40] S. M. Albrecht, E. B. Hansen, A. P. Higginbotham, F. Kuemmeth, T. S. Jespersen, J. Nygård, P. Krogstrup, J. Danon, K. Flensberg, and C. M. Marcus, Transport Signatures of Quasiparticle Poisoning in a Majorana Island, *Phys. Rev. Lett.* **118**, 137701 (2017).
- [41] D. Rainis and D. Loss, Majorana qubit decoherence by quasiparticle poisoning, *Phys. Rev. B* **85**, 174533 (2012).
- [42] P. P. Aseev, J. Klinovaja, and D. Loss, Lifetime of Majorana qubits in Rashba nanowires with non-uniform chemical potential, *Phys. Rev. B* **98**, 155414 (2018).
- [43] P. Schüffelgen *et al.*, Selective area growth and stencil lithography for in situ fabricated quantum devices, *Nat. Nanotechnol.* **14**, 825 (2019).
- [44] A. Matos-Abiague, J. Shabani, A. D. Kent, G. L. Fatin, B. Scharf, and Žutić, Tunable magnetic textures: From Majorana bound states to braiding, *Solid State Commun.* **262**, 1 (2017).
- [45] P. Wei, S. Manna, M. Eich, P. Lee, and J. Moodera, Superconductivity in the Surface State of Noble Metal Gold and its Fermi Level Tuning by EuS Dielectric, *Phys. Rev. Lett.* **122**, 247002 (2019).
- [46] M. Kjaergaard, K. Wölms, and K. Flensberg, Majorana fermions in superconducting nanowires without spin-orbit coupling, *Phys. Rev. B* **85**, 020503(R) (2012).
- [47] N. Mohanta, T. Zhou, J. W. Xu, J. E. Han, A. D. Kent, J. Shabani, I. Žutić, and A. Matos-Abiague, Electrical Control of Majorana Bound States Using Magnetic Stripes, *Phys. Rev. Applied* **12**, 034048 (2019).
- [48] M. M. Desjardins, L. C. Contamin, M. R. Delbecq, M. C. Dartailh, L. E. Bruhat, T. Cubaynes, J. J. Viennot, F. Mallet, S. Rohart, A. Thiaville, A. Cottet, and T. Kontos, Synthetic spin-orbit interaction for Majorana devices, *Nat. Mater.* **18**, 1060 (2019).
- [49] A. Yazdani, Conjuring Majorana with synthetic magnetism, *Nat. Mater.* **18**, 1036 (2019).
- [50] P. Virtanen, F. S. Bergeret, E. Strambini, F. Giazotto, and A. Braggio, Majorana bound states in hybrid two-dimensional Josephson junctions with ferromagnetic insulators, *Phys. Rev. B* **98**, 020501(R) (2018).
- [51] S. K. Kim, S. Tewari, and Y. Tserkovnyak, Control and braiding of Majorana fermions bound to magnetic domain walls, *Phys. Rev. B* **92**, 020412(R) (2015).
- [52] P. Marra and M. Cuoco, Controlling Majorana states in topologically inhomogeneous superconductors, *Phys. Rev. B* **95**, 140504(R) (2017).
- [53] U. Güngördu, S. Sandhoefer, and A. A. Kovalev, Stabilization and control of Majorana bound states with elongated Skyrmions, *Phys. Rev. B* **97**, 115136 (2018).
- [54] G. Yang, P. Stano, J. Klinovaja, and D. Loss, Majorana bound states in magnetic Skyrmions, *Phys. Rev. B* **93**, 224505 (2016).

- [55] A. Palacio-Morales, E. Mascot, S. Cocklin, H. Kim, S. Rachel, D. K. Morr, and R. Wiesendang, Atomic-scale interface engineering of Majorana edge modes in a 2D magnet-superconductor hybrid system, *Sci. Adv.* **5**, eaav6600 (2019).
- [56] S. Boutin, J. Camirand Lemyre, and I. Garate, Majorana bound state engineering via efficient real-space parameter optimization, *Phys. Rev. B* **98**, 214512 (2018).
- [57] J. Alicea, Y. Oreg, G. Refael, F. von Oppen, and M. P. A. Fisher, Non-Abelian statistics and topological quantum information processing in 1D wire networks, *Nat. Phys.* **7**, 412 (2011).
- [58] J. Klinovaja and D. Loss, Time-reversal invariant parafermions in interacting Rashba nanowires, *Phys. Rev. B* **90**, 045118 (2014).

SUPPLEMENTAL MATERIAL

Phase Control of Majorana Bound States in a Topological X Junction

Tong Zhou^{1,*}, Matthieu C. Dartailh², William Mayer², Jong E.
Han¹, Alex Matos-Abiague³, Javad Shabani², and Igor Žutić^{1†}

¹*Department of Physics, University at Buffalo, State University of New York, Buffalo, New York 14260, USA*

²*Center for Quantum Phenomena, Department of Physics, New York University, New York 10003, USA*

³*Department of Physics and Astronomy, Wayne State University, Detroit, Michigan 48201, USA*

I. MAJORANA BOUND STATES IN A SINGLE PLANAR JOSEPHSON JUNCTION WITH ROTATED IN-PLANE MAGNETIC FIELD

Here we provide discussion about the results of the Majorana bound states (MBS) in a single planar Josephson junction (JJ) with rotated in-plane magnetic field, \mathbf{B} . Such a single JJ can be viewed as a special case of the X-shaped junction (XJ) when the two superconducting (S) regions are parallel, as shown in Fig. S1(a). Equivalently, this corresponds to the central angle $2\theta = 0$, defined between the two S regions in the Fig. 1 of the main text. Previous publications have reported that the topological superconductivity in planar JJs exists over a large parameter space when the magnetic field is along the S/normal region (N) interface [1–4]. Here we explore how the MBS evolve for in-plane B-field at a misalignment angle β with the S/N interface, introduced in Fig. S1(a). The corresponding Bogoliubov-de Gennes (BdG) Hamiltonian for the single JJ is the same as from the Eq. (1) in main text, but with the pairing potential, $\Delta(x)$, and chemical potential, $\mu(x)$, having one-dimensional dependences, written as

$$H = \left[\frac{\mathbf{p}^2}{2m^*} - \mu(x) + \frac{\alpha}{\hbar} (p_y \sigma_x - p_x \sigma_y) \right] \tau_z - \frac{g^* \mu_B}{2} \mathbf{B} \cdot \boldsymbol{\sigma} + \Delta(x) \tau_+ + \Delta^*(x) \tau_-, \quad (1)$$

where \mathbf{p} is the momentum, α is the Rashba spin-orbit coupling (SOC) strength, \mathbf{B} is the external magnetic field, μ_B is the Bohr magneton, while m^* and g^* are the electron effective mass and g -factor, respectively, taken a $m^* = 0.03m_0$,

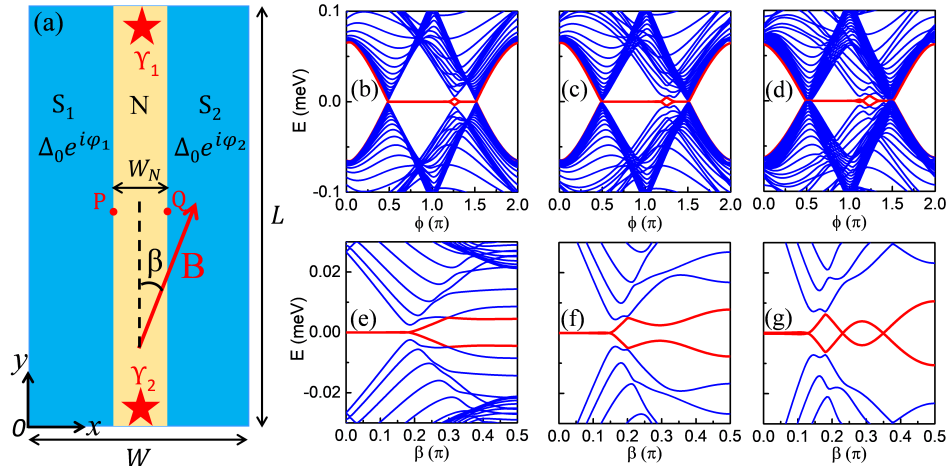


Fig. S 1. (a) Schematic of a planar Josephson junction with in-plane magnetic field, \mathbf{B} , at a misalignment angle β with the superconductor/normal region (S/N) interface. Two MBS, γ_1 and γ_2 , are denoted by stars at the opposite ends of the N region. P and Q denote the closest points at the edge of the opposite S regions, subsequently shown also in the X-shaped junctions. (b)-(d) Energy spectra with $B = 0.4$ T as a function of the superconducting phase difference, $\phi = \varphi_1 - \varphi_2$, for β of 0, 0.1π , and 0.15π , respectively. (e)-(g) Energy spectra as a function of the angle β with the phase difference of $\phi = \pi$ for $B = 0.2$ T, 0.4 T, and 0.6 T, respectively. The red lines in the spectra indicate the evolution of finite-energy states into MBS inside the topological gap. The spectra were obtained for a junction with length $L = 3.2$ μm , width $W = 1.6$ μm and $W_N = 100$ nm. The other parameters are the same as those in the Fig. 2. of the main text.

* tzhou8@buffalo.edu

† zigor@buffalo.edu

where m_0 is the electron mass, and $g^* = 10$ for InAs. We use τ_i (σ_i) as the Nambu (Pauli) matrices in particle-hole (spin) space and $\tau_{\pm} = (\tau_x \pm \tau_y)/2$. For the Zeeman term, we can write $\mathbf{B} \cdot \boldsymbol{\sigma} = \sigma_y B \cos \beta + \sigma_x B \sin \beta$ and the proximity-induced superconducting pairing potential for the 2DEG below the S leads,

$$\Delta(x) = \begin{cases} \Delta_0 \sqrt{1 - (B/B_c)^2} e^{i\varphi_1/2} & \text{for } 0 < x < (W - W_N)/2, \\ 0 & \text{for } (W - W_N)/2 \leq x \leq (W + W_N)/2, \\ \Delta_0 \sqrt{1 - (B/B_c)^2} e^{i\varphi_2/2} & \text{for } (W + W_N)/2 < x < W, \end{cases} \quad (2)$$

is expressed in terms of Δ_0 the superconducting gap, B_c the critical magnetic field, and the geometric parameters depicted in Fig. S1. For proximity-induced superconductivity in InAs we take $\Delta_0 = 0.23$ meV and $B_c = 1.6$ T for Al.

Solving the BdG Hamiltonian, we get the phase-difference biased energy spectra for different B-field orientation β , as shown in Fig. S1(b)-(d). As expected, the MBS emerge when $\beta = 0$ [Fig. S1(b)], in agreement with the previous work [1–4]. When β is increased, the phase-difference range supporting MBS becomes smaller [Figs. S1(c) and (d)]. However, even when β is up to 0.15π , there is still a large range of the phase difference (0.58π to 1.16π) supporting topological states [Fig. S1(d)]. To explore the range of β supporting MBS, we plot the β -dependent energy spectra of π -JJ in Fig. S1(e)-(g) for different values of magnetic field. As the misalignment angle increases, one can see the topological region is reduced and, eventually, fully suppressed, as observed experimentally [4]. However, the MBS would still survive for $B = 0.2$ T when the value of the misalignment angle is up to 0.2π , providing a useful guidance in designing XJs.

II. SUPERCONDUCTING AND NORMAL REGIONS IN X JUNCTIONS

By choosing the origin of the coordinate system at the lower-left corner, as shown in Fig. S2(a), for the proximity-induced superconductivity in a two-dimensional electron gas (2DEG), covered by an s -wave superconductor, we can describe four superconducting regions (S_1 , S_2 , S_3 , and S_4) and a normal region (N), uncovered by the superconductor, by the following relations,

$$\begin{aligned} S_1(x, y) &= \begin{cases} y > \cot \theta (x - x_P) + y_P \\ y > -\cot \theta (x - x_Q) + y_Q \end{cases}, & S_2(x, y) &= \begin{cases} y < \cot \theta (x - x_Q) + y_Q \\ y > -\cot \theta (x - x_P) + y_P \end{cases}, \\ S_3(x, y) &= \begin{cases} y < -\cot \theta (x - x_P) + y_P \\ y < \cot \theta (x - x_Q) + y_Q \end{cases}, & S_4(x, y) &= \begin{cases} y > \cot \theta (x - x_P) + y_P \\ y < -\cot \theta (x - x_P) + y_P \end{cases}, \end{aligned} \quad (3)$$

$$N(x, y) = \begin{cases} y \geq \cot \theta (x - x_Q) + y_Q \\ y \leq \cot \theta (x - x_P) + y_P \end{cases} \text{ or } \begin{cases} y \geq -\cot \theta (x - x_P) + y_P \\ y \leq -\cot \theta (x - x_Q) + y_Q \end{cases}, \quad (4)$$

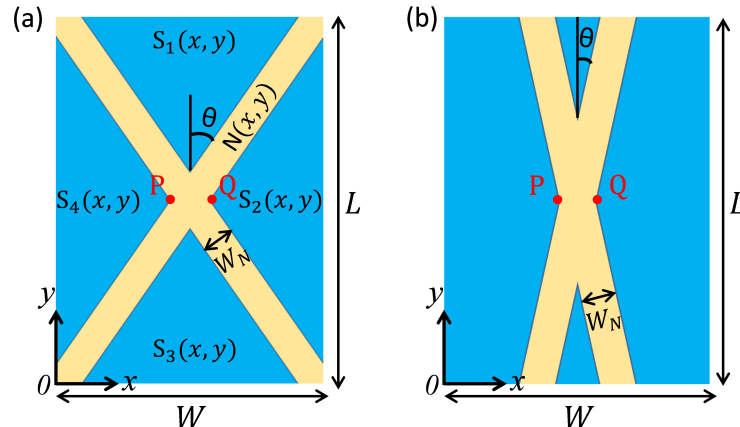


Fig. S 2. (a) Schematic of the XJ with position functions. P and Q points are the fixed crossing points. $S_1(x, y)$, $S_2(x, y)$, $S_3(x, y)$, $S_4(x, y)$, and $N(x, y)$ are the algebraic descriptions for S_1 , S_2 , S_3 , S_4 , and N regions, respectively. (b) Schematic of the XJ with the angle θ close to zero ($\tan \theta \ll W/L$).

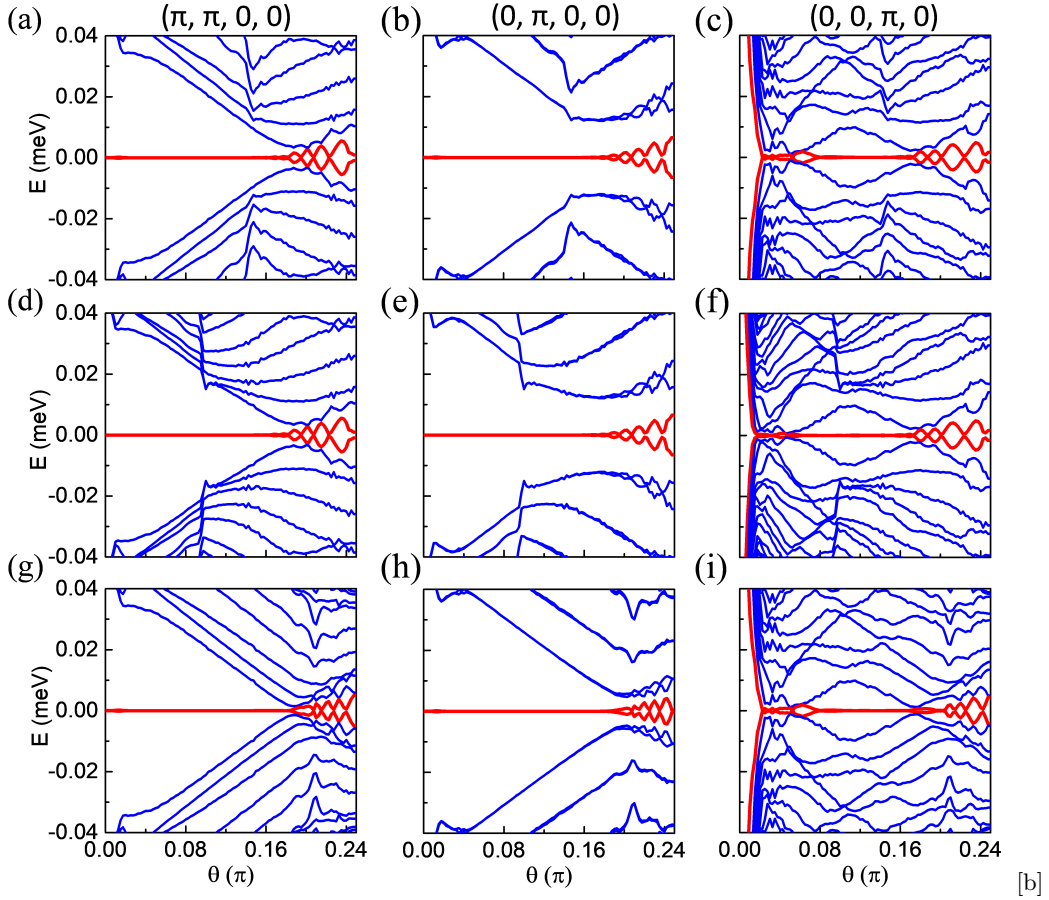


Fig. S 3. (a)-(c) Calculated energy spectra as a function of the central angle 2θ in XJs with $B = 0.4$ T for the diagonal $(\pi, \pi, 0, 0)$, long-edge $(0, \pi, 0, 0)$, and short-edge $(0, 0, \pi, 0)$ MBS types, respectively. The red lines indicate the evolution of the finite-energy states into MBS inside the topological gap. The geometric parameters are $L = 3.2 \mu\text{m}$, $W = 1.6 \mu\text{m}$, and $W_N/\cos\theta = 100 \text{ nm}$. The other parameters, which are taken from Fig. 2 in main text. (d)-(f), are same as in panels (a)-(c), but with $L = 4.8 \mu\text{m}$. The parameters from panels (g)-(i) are the same as those in (a)-(c), but with $W = 2.4 \mu\text{m}$.

where (x_P, y_P) and (x_Q, y_Q) are the coordinates of the points P and Q , with $x_P = (W - W_N/\cos\theta)/2$, $x_Q = (W + W_N/\cos\theta)/2$, and $y_P = y_Q = L/2$. When θ is changed, the distance between the points P and Q points is fixed, but W_N varies, see Fig. S2(b). In the limiting case when θ is zero, the XJ becomes a single JJ, as shown in Fig. S1(a).

III. GEOMETRICAL EFFECTS IN X JUNCTIONS

In this Section we explore how the geometric parameters affect the MBS formation in XJs, especially as the central angle, 2θ , is changed. With the fixed system size, $L = 3.2 \mu\text{m}$, $W = 1.6 \mu\text{m}$, and $PQ = W_N/\cos\theta = 100 \text{ nm}$, the distance between the crossing points, P and Q , we plot θ -dependent energy spectra in Fig. S3(a)-(c) for the diagonal, long-edge, and short-edge MBS types, respectively. When $\theta \sim 0$, the diagonal and long-edge configuration can be approximated by a single π -JJ where the MBS are stable for a large range of parameters [1–4]. Therefore MBS emerge in XJs as expected from the previously studied planar JJs, as shown in Figs. S3(a) and S3(b).

When θ is increased, the misalignment between the B-field along the y-direction and the S/N interface becomes larger. As a result of these less-favorable conditions, the MBS become fragile, which is consistent with the enhanced MBS oscillations. However, when θ is smaller than 0.18π , the MBS are stable for both configurations. Thus, the range of θ supporting diagonal and long-edge MBS are from 0 to 0.18π . For short-edge MBS, when $\theta \sim 0$, the areas of S_1 and S_3 are too small to support such MBS [see Fig. S2(b)]. As shown in Fig. S3(c), the MBS do not emerge until θ reaches 0.08π and become unstable when $\theta \approx 0.18\pi$. Thus, the range of θ supporting short-edge MBS is from 0.08π to 0.18π .

We also explore the influence of the system size of XJs. As shown in Fig. S3(d)-(i), increasing the XJ's length (L)

and width (W) does not give a clear change for all the three types of MBS (slightly suppress the oscillations of the zero-energy bands for short-edge MBS), indicating that the system size with $L \geq 3.2 \mu\text{m}$ and $W \geq 1.6 \mu\text{m}$ is already large enough to support MBS. With these results, we can identify that all the three MBS types can coexist in a robust form for θ from 0.08π to 0.18π with $L \geq 3.2 \mu\text{m}$ and $W \geq 1.6 \mu\text{m}$. Such a large parameter range gives a considerable flexibility for XJ fabrication. In fact the size of our fabricated XJ [see Fig. 1(b) in the main text] already fits well in this range of suitable geometric parameters, with $L = 4.0 \mu\text{m}$, $W = 2.0 \mu\text{m}$ and $\theta = 0.15\pi$.

IV. MBS EXCHANGE IN X JUNCTIONS

In this Section we provide complementary information about the MBS exchange by controlling the phase differences among the four S regions ($\varphi_1, \dots, \varphi_4$) with external fluxes Φ_1, Φ_2 , and Φ_3 , depicted in Fig. 1. In Figs. 3(f)-(j), we have shown the evolution of the calculated MBS probability densities from the diagonal [Fig. 3(a)] to a long-edge MBS [Fig. 3(b)] through continuously changing φ_1 from π to 0, but fixing $\varphi_2 = \pi$, $\varphi_3 = 0$, and $\varphi_4 = 0$ with external magnetic flux control. For this MBS evolution depicted in Fig. S4(a), we provide the corresponding low-energy spectra in Fig. S4(b). For any value of the continuously changing φ_1 , the MBS are protected by the topologically-nontrivial superconducting gap and remain stable during the whole switching time. As a result, the γ_2 can be adiabatically moved from the upper-left to the upper-right corner through the XJ center. We also provide an animation (see Diagonal2long.GIF) to show the whole process of the evolution of the MBS probability density for Fig. S4(a). Because of the XJ symmetry, the low-energy spectra of the evolution from long-edge MBS [Fig. 3(b)] to the other diagonal MBS [Fig. 3(c)] is same as that already shown in Fig. S4(b).

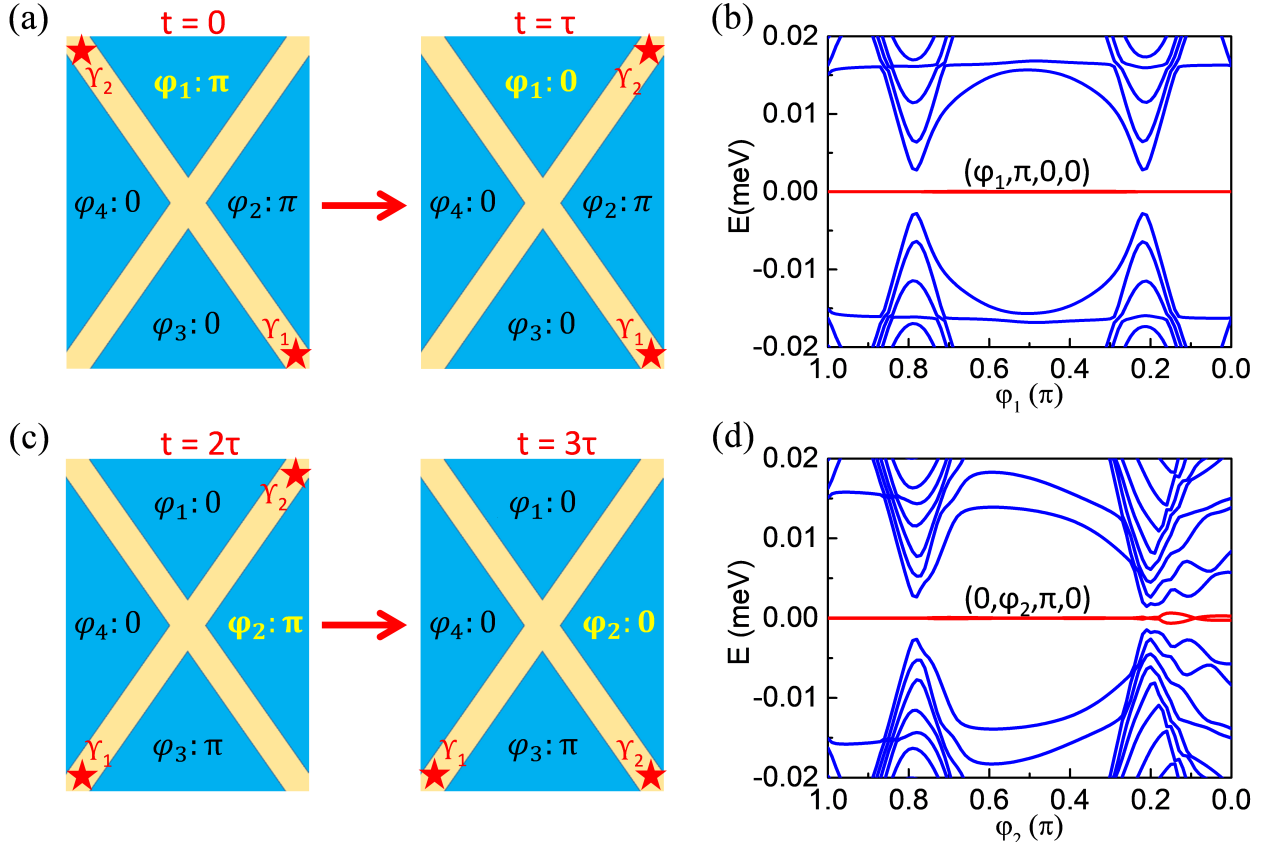


Fig. S 4. (a) Schematic of the evolution from the diagonal MBS [Fig. 3(a)] with $(\varphi_1, \varphi_2, \varphi_3, \varphi_4) = (\pi, \pi, 0, 0)$ to a long-edge MBS [(Fig. 3(b))] with $(\varphi_1, \varphi_2, \varphi_3, \varphi_4) = (0, \pi, 0, 0)$. (b) The corresponding calculated spectra for (a) with continuously changing φ_1 from π to 0, but fixing $\varphi_2 = \pi$, $\varphi_3 = 0$, and $\varphi_4 = 0$. (c) Schematic of the evolution from the diagonal MBS [Fig. 3(c)] with $(\varphi_1, \varphi_2, \varphi_3, \varphi_4) = (0, \pi, \pi, 0)$ to a short-edge MBS [Fig. 3(d)] with $(\varphi_1, \varphi_2, \varphi_3, \varphi_4) = (0, 0, \pi, 0)$. (d) The corresponding calculated spectra for (c) with continuously changing φ_2 from π to 0, but fixing $\varphi_1 = 0$, $\varphi_3 = \pi$, and $\varphi_4 = 0$. The parameters are taken from Fig. 2.

We also provide a similar analysis for another step in the MBS exchange which is shown schematically in Fig. S4(c) as the evolution from the diagonal MBS [Fig. 3(c)] to a short-edge MBS [Fig. 3(d)] through continuously changing φ_2 from π to 0, but fixing $\varphi_1 = 0$, $\varphi_3 = \pi$, and $\varphi_4 = 0$. The corresponding evolution of the low-energy spectra is given in Fig. S4(d). Similar as in the previous step of the MBS exchange, for any value of the continuously changing φ_2 , the MBS are protected by the topologically-nontrivial superconducting gap and remain stable during the switching time. We provide the animation (see Diagonal2short.GIF) for the whole process of the evolution of the MBS probability density for Fig. S4(c). Invoking the XJ symmetry, the low-energy spectra of the evolution from Fig. 3(d) to Fig. 3(e) is same as shown Fig. S4(d), indicating that the short-edge MBS [Fig. 3(d)] can be adiabatically changed into the diagonal MBS [Fig. 3(e)]. These additional results and discussion corroborate that MBS in XJs can indeed be flexibly manipulated by the external flux control.

To realize the adiabatic evolution of the MBS exchange in Fig. 3, the switching time, τ , should be larger than the time τ_u , expected from the uncertainty relation, $\Delta E \tau_u \sim \hbar/2$, where ΔE is the energy gap between the ground state and first excited state. From our calculations in Fig. S4, the smallest ΔE is about $2 \mu\text{eV}$ during the whole process of MBS exchange, giving an estimated τ_u of approximately 0.17 ns. Thus, the switching time should exceed 0.17 ns to realize the adiabatic MBS evolution.

On the other hand, to avoid the quasiparticle poisoning, the switching time should be smaller than the quasiparticle poisoning time of the MBS, τ_p , in XJs. While, to the best of our knowledge, there are still no experimental measurements of τ_p in planar JJs, such τ_p is well explored in nanowire systems [5–7]. Specifically, $\tau_p \sim 1 \mu\text{s}$ is experimentally reported in Al/InAs system [5]. Considering that we analyze the same materials system, for the operation of XJs we also used $\tau_p \sim 1 \mu\text{s}$. Therefore, with $0.17 \text{ ns} < \tau < 1 \mu\text{s}$ we can apply the considered analysis to exchange the MBS in our XJ. Such condition on the relevant timescales can be readily achieved with external flux control, which eliminates the risk of excitation from the ground state and quasiparticle poisoning during the switching.

V. MBS FUSION IN X JUNCTIONS

In this Section, we show that XJs can be used to implement the fusion of MBS, which is an important step in demonstrating the non-Abelian character of MBS [8]. Figure S5(a) provides the flux protocol and the phase control for the fusion of the MBS. As shown schematically in Figs. S5(b)-(f), the diagonal MBS can be gradually moved and fused at the center of the XJ using the three external fluxes to change Φ_1 from 0 to $-0.25\Phi_0$ and then to change Φ_2 from $0.5\Phi_0$ to $0.25\Phi_0$ and Φ_3 from 0 to $0.25\Phi_0$, simultaneously, within the time 2τ , as shown in Fig. S5(a). Since we have shown in Fig. 4 of the main text that 4 MBS can be generated, a more complex fusion in XJ, for example, fusing (γ_1, γ_2) by changing φ_1 from π to 0 and fusing (γ_2, γ_3) by changing φ_2 from 0 to π can access different fusion channels, which could probe non-Abelian statistics [8].

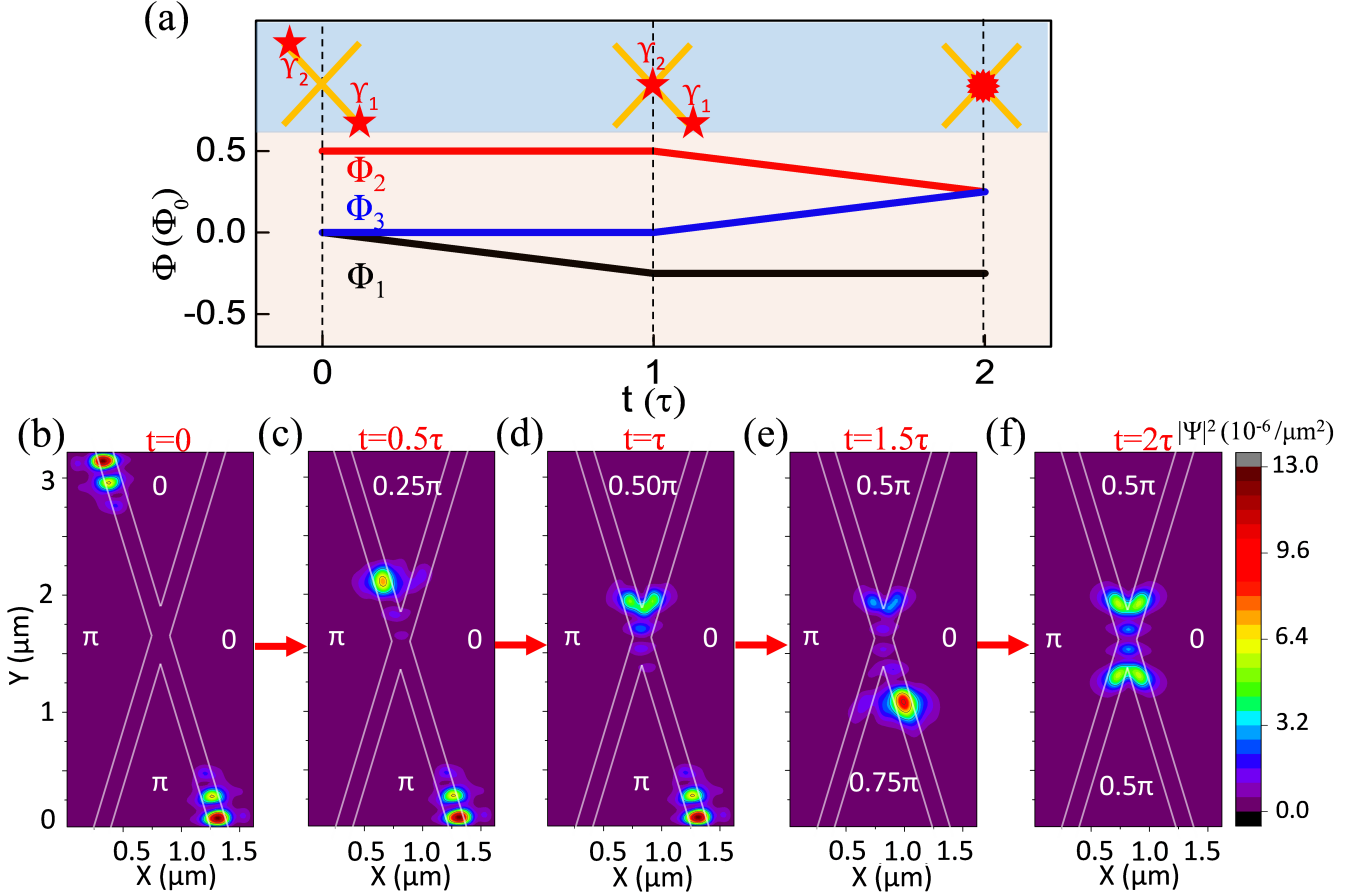


Fig. S 5. (a) Schematic of the flux protocol for the MBS fusion with external fluxes, τ is the switching time and Φ_0 is the magnetic flux quantum. (b) - (f) Calculated MBS probability densities for the MBS fusion. The parameters are taken from Fig. 3.

-
- [1] F. Pientka, A. Keselman, E. Berg, A. Yacoby, A. Stern, and B. I. Halperin, Phys. Rev. X **7**, 021032 (2017).
[2] H. Ren, F. Pientka, S. Hart, A. Pierce, M. Kosowsky, L. Lunczer, R. Schlereth, B. Scharf, E. M. Hankiewicz, L. W. Molenkamp, B. I. Halperin, and A. Yacoby, Nature **569**, 93 (2019).
[3] A. Fornieri, A. M. Whiticar, F. Setiawan., E. Portolés, A. C. C. Drachmann, A. Keselman, S. Gronin, C. Thomas, T. Wang, R. Kallaher, G. C. Gardner, E. Berg, M. J. Manfra, A. Stern, C. M. Marcus, and F. Nichele, Nature **569**, 89 (2019).
[4] W. Mayer, M. C. Dartiailh, J. Yuan, K. S. Wickramasinghe, A. Matos-Abiague, I. Žutić, and J. Shabani, arXiv:1906.01179 (2019).
[5] S. M. Albrecht, E. B. Hansen, A. P. Higginbotham, F. Kuemmeth, T. S. Jespersen, J. Nygård, P. Krogstrup, J. Danon, K. Flensberg, and C. M. Marcus, Phys. Rev. Lett. **118**, 137701 (2017).
[6] D. Rainis and D. Loss, Phys. Rev. B **85**, 174533 (2012).
[7] P. Aseev, J. Klinovaja, and D. Loss, Phys. Rev. B **98**, 155414 (2018).
[8] D. Aasen, M. Hell, R. V. Mishmash, A. Higginbotham, J. Danon, M. Leijnse, T. S. Jespersen, J. A. Folk, C. M. Marcus, K. Flensberg, and J. Alicea, Phys. Rev. X **6**, 031016 (2016).